New Journal of Physics
The open access journal at the forefront of physics

Deutsche Physikalische Gesellschaft DPG
IOP Institute of Physics

Published in partnership with: Deutsche Physikalische Gesellschaft and the Institute of Physics

OPEN ACCESS

RECEIVED
15 March 2019

REVISED
21 May 2019

ACCEPTED FOR PUBLICATION
21 June 2019

PUBLISHED
8 July 2019

PAPER

Formation of antihydrogen beams from positron–antiproton interactions

S Jonsell [1,3] and M Charlton [2]

[1] Department of Physics, Stockholm University, SE-10691 Stockholm, Sweden
[2] Department of Physics, College of Science, Swansea University, Swansea SA2 8PP, United Kingdom
[3] Author to whom any correspondence should be addressed.

E-mail: jonsell@fysik.su.se **and** m.charlton@swansea.ac.uk

Keywords: antihydrogen, antiprotons, beams, positron, plasma

Abstract

The formation of a beam of antihydrogen atoms when antiprotons pass through cold, dense positron plasmas is simulated for various plasma properties and antiproton injection energies. There are marked dependences of the fraction of injected antiprotons which are emitted as antihydrogen in a beam-like configuration upon the temperature of the positrons, and upon the antiproton kinetic energy. Yields as high as 13% are found at the lowest positron temperatures simulated here (5 K) and at antiproton kinetic energies below about 0.1 eV. By 1 eV the best yields are as low as 10^{-3}, falling by about two orders of magnitude with an increase of the positron temperature to 50 K. Example distributions for the antihydrogen angular emission, binding energy and kinetic energy are presented and discussed. Comparison is made with experimental information, where possible.

1. Introduction

Over the past few years the first quantitative tests of matter–antimatter symmetry using antihydrogen ($\bar{\mathrm{H}}$) have been achieved by the ALPHA collaboration, including measurements based upon 1s–2s spectroscopy [1], via observation of the Lyman-α transition [2] and involving hyperfine transitions [3]. These, and other, advances were made possible by the confinement of $\bar{\mathrm{H}}$ in magnetic minimum traps [4–6]. Recently, these techniques have been improved at CERN's antiproton decelerator (AD) [7] such that about 10–20 $\bar{\mathrm{H}}$s can be trapped per antiproton ($\bar{p}$) bunch, and through the accumulation of $\bar{\mathrm{H}}$s from successive bunches [8] several hundred $\bar{\mathrm{H}}$s can be held simultaneously [2].

Other AD experiments, namely ASACUSA [9], AEGIS [10] and GBAR [11], aim to create, and make measurements using, beams of $\bar{\mathrm{H}}$ atoms. One advantage of this approach is that the investigations can be performed in a field-free region, thus avoiding the Zeeman and motional Stark shifts that are inevitable in a magnetic trap environment. Two methods are being pursued to achieve useful $\bar{\mathrm{H}}$ beams: AEGIS and GBAR seek to create the $\bar{\mathrm{H}}$s by charge exchange with excited Ps atoms [12], while ASACUSA uses the same three-body $\bar{\mathrm{H}}$ formation processes (i.e. $e^+ + e^+ + \bar{p} \rightarrow \bar{\mathrm{H}} + e^+$, which involves $\bar{p}$ interactions with cold, dense positron (e^+) plasmas) as utilised by ALPHA and ATRAP. The ASACUSA experiment has succeeded in detecting $\bar{\mathrm{H}}$ at a distance 2.7 m downstream from the production region, after injecting a bunch of $\bar{p}$s from the AD into their e^+ plasma [9]. In this experiment $\bar{p}$s that did not form $\bar{\mathrm{H}}$ on the first pass through the positrons were reflected back through the plasma, thus allowing several attempts to form the anti-atom. Whilst such an approach will enhance the $\bar{\mathrm{H}}$ yield, it is however likely to increase the spread in $\bar{\mathrm{H}}$ velocities, resulting in a less well-defined beam. In this communication we mostly treat the situation of a single $\bar{p}$ pass through the positrons and we note that, with the larger numbers of trapped $\bar{p}$ available with the upcoming ELENA ring [13], it may become possible to create a usable $\bar{\mathrm{H}}$ beam using a tailored single pass approach.

In a previous publication we investigated mechanisms for radial transport of $\bar{p}$s inside a positron plasma held in a Penning trap [14]. We found that the dominant transport mechanism arises from a combination of $\bar{\mathrm{H}}$ formation and the circular drift motion of $\bar{p}$s in the particle trap. More recently, we studied the consequences of

this radial transport for the number of trappable $\bar{H}$ atoms generated in an experimental situation typical of ALPHA or ATRAP [15]. The purpose of the present paper is to investigate how the radial transport affects the number of beam-like $\bar{H}$s generated from three-body combination of antiprotons injected in a positron plasma. Similar studies have been reported previously [16–18], but none of these have explicitly included the $\bar{p}$ and $\bar{H}$ velocity, and hence their radial transport, in the simulations. Instead rate equations were solved for a stationary $\bar{p}$, in order to evaluate the $\bar{H}$ yield. In [17, 18], the axial $\bar{p}$ velocity was accounted for by limiting the evolution time to the plasma length divided by the initial $\bar{p}$ axial speed. In [18] the $\bar{H}$s generated were further assigned velocities given by a simplified description of the distributions resulting from simulations reported in [19]. However, neither of these approaches takes proper account of the complex interplay between transport processes and the gradual accumulation of binding energy in a series of collisions. Elucidation of these aspects is the main purpose of the present paper, the remainder of which is organised as follows. In section 2 we give a brief description of our methodology, with particular emphasis on the differences between that applied here and our previous work, including our working definition of an antihydrogen beam, and this is followed by the main results and accompanying discussion in section 3 and our conclusions in section 4.

2. Method

The details of our simulation method have been published in [14]. Briefly, we calculate classical trajectories of antiprotons and positrons, using the full equations of motion in the combination of magnetic and electric (self charge of the positron plasma) fields. Stable $\bar{H}$s are defined as those that survive 1 μs in an axial 10 V cm^{-1} electric field after leaving the plasma. The main differences from [14] are: (i) the positron plasma is modelled as a cylinder with a finite length (usually 1 cm in the work reported here), and the $\bar{p}$s make a single pass through this plasma; (ii) the $\bar{p}$s are initialised with a finite injection energy ($E_{\rm in}$) in the axial direction, while thermal with the plasma temperature in the transverse direction (the transverse degrees of freedom typically thermalise quickly [20]), and (iii) no filtering is made on the final magnetic moment or kinetic energy of the $\bar{H}$, instead our main observable is the angular deviation α between the velocity vector of the emerging $\bar{H}$ and the Penning trap axis (which is taken as the required direction of the beam). In contrast to [16–18] we do not include radiative processes (which have a negligible contribution in the initial stages of $\bar{H}$ formation, and on the few μs timescale relevant here). Thus, the binding energy is followed only as long as the $\bar{H}$ remains in the plasma and evolves, after an initial three-body recombination event, through successive collisions with the positrons. Such collisions can both increase and reduce the binding of an $\bar{H}$ atom. If the $\bar{H}$ is ionised whilst inside the plasma, the liberated antiproton may undergo another three-body recombination event before exiting the plasma. Due to radial transport processes, it is important to note that $\bar{H}$ may also exit the plasma radially, i.e. through the mantle of the cylindrical plasma.

All of the simulations presented here are for axial magnetic fields of 1 or 3 T. We have investigated four different temperatures, T_e, of the positron plasma (5, 15, 30 and 50 K), with the latter modelled as a cylinder of uniform density, and with a radius of 1 mm. Except where we specify otherwise the length of the plasma was taken to be $l = 1$ cm. In most cases we have assumed a relatively high plasma density, $n_e = 10^{15}$ m^{-3}, which is likely to enhance $\bar{H}$ formation, and hence promote beam formation. (Note that, in the simulations described in [16] densities between 10^{14} m^{-3} and 10^{16} m^{-3} were used.) Whilst we have also explored down to 10^{14} m^{-3}, we have not tried to increase beyond 2×10^{15} m^{-3}. This is because at very large densities, there is a mismatch between the drift velocities of $\bar{p}$s and positrons, in contrast to the situation at moderate densities where both particle species rotate with the same angular velocity. Thus, at very large densities, and away from the axis of the trap, positrons and $\bar{p}$s will not share a common reference frame, but will on average have a large relative velocity, which will reduce the probability of antihydrogen formation. Reductions are likely to be exacerbated for beam-like antihydrogen, because of the large velocity component in the transverse direction. For most of our simulations the $\bar{p}$ were initialised on the axis of the trap, $\rho_{\rm start} = 0$, and parallel to it, and with an energy between 0.004 eV (corresponding to 50 K in temperature units) and 1 eV.

In the main, we analyse two quantities: (i) the $\bar{H}$ fraction, $f_{\bar{H}}$, i.e. the fraction of $\bar{p}$s entering the positrons that have been converted to stable (according to the definition above) $\bar{H}$ upon leaving the plasma (either at the other end of the plasma, or through its mantle), and (ii) the beam fraction, $f_{\rm beam}$, i.e. the same, but with the additional criterion that the divergence of the velocity from the axis satisfies $\tan\alpha < 0.1$. This is a pragmatic choice which, experimentally, may be manageable if focussing elements can be used to steer the divergent flux (see, e.g. the experimental arrangement discussed for an antihydrogen beam experiment by Sauerzopf and co-workers [21]) and which also allows us to obtain statistically significant samples over the range of parameters we have explored.

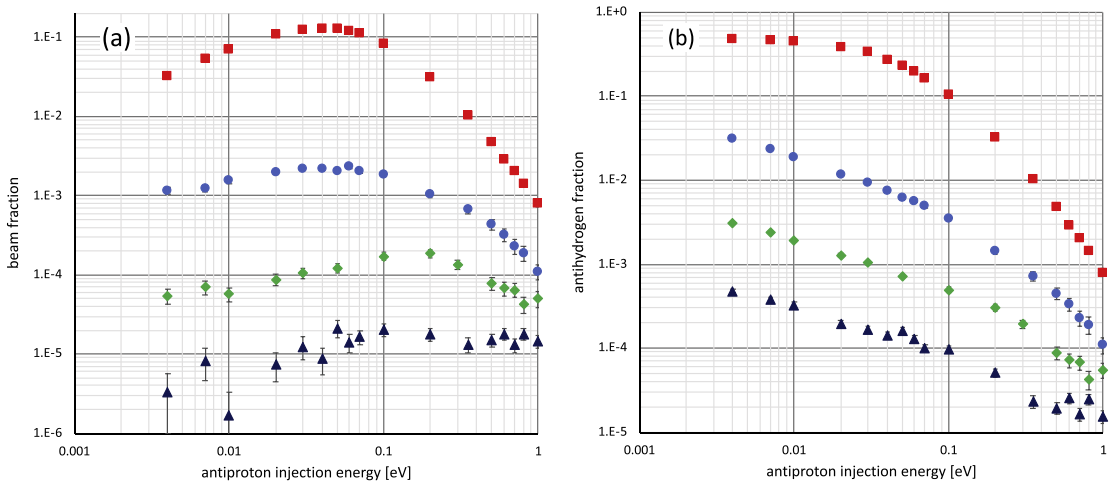

Figure 1. Panel (a): the fraction of $\bar{p}$s converted to beam-like $\bar{\mathrm{H}}$ (see text) after traversing a 1 cm long positron plasma with density $n_e = 10^{15}$ m^{-3}, as a function of their initial kinetic energy. Panel (b): the corresponding $\bar{\mathrm{H}}$ fraction. In both (a) and (b) the data are for different values of the positron plasma temperature as $T_e = 5$ K (red squares), 15 K (blue circles), 30 K (green diamonds) and 50 K (black triangles). The axial magnetic field was $B = 1$ T, the radius of the plasma was 1 mm, its length 1 cm and the $\bar{p}$s were injected on the axis of the trap.

3. Results and discussion

Our main results, the beam fraction for $\bar{p}$s injected on the axis of the trap with different injection energies, and traversing, in a single pass, positron plasmas held at various T_e are summarised in figure 1(a). As expected, this fraction is enhanced with reduced T_e, owing to the increased collision rate. A more unexpected feature is the maximum around an injection energy of $E_{\mathrm{in}} \simeq 0.05$ eV. The largest simulated f_{beam} obtained for a 5 K plasma is 13%, while for a three times higher T_e the maximum drops by nearly two orders of magnitude to 0.2%. Additional moderate increases in T_e give further order of magnitude drops.

Figure 1(b) shows $f_{\bar{\mathrm{H}}}$ for the same set of parameters. For large E_{in} the number of $\bar{\mathrm{H}}$ generated drops, because the $\bar{p}$s have less time to undergo a three-body recombination process, and any loosely bound $\bar{\mathrm{H}}$s formed do not have time to undergo enough stabilising collisions with positrons, before leaving the plasma. There is no evidence for a local maximum at any E_{in}. Hence, we conclude that the feature in figure 1(a) is the combined effect of the drop in $f_{\bar{\mathrm{H}}}$ at high energies, and the reduced axial velocity at low energies, which results in a more isotropic, hence not beam-like, shower of $\bar{\mathrm{H}}$s leaving the positron plasma. We further note that at 1 eV, the highest injection energy investigated here, $f_{\bar{\mathrm{H}}} \simeq f_{\mathrm{beam}}$, meaning that all $\bar{\mathrm{H}}$ formed are part of the beam. However, in the same limit the fraction of $\bar{p}$s converted to $\bar{\mathrm{H}}$s is markedly reduced. The reduction of $f_{\bar{\mathrm{H}}}$ with plasma temperature mirrors that of f_{beam}, which is thus explained by a lower formation rate for $\bar{\mathrm{H}}$.

Next, we investigate our assumption that the $\bar{p}$s are injected on the trap axis, and figure 2 shows the effect, at $T_e = 15$ K, of moving slightly off axis (with the $\bar{p}$ injected at a radial distance of $\rho = 0.1$ mm). At low E_{in}, f_{beam} drops from its on-axis value of 0.1%–0.2% by about an order of magnitude to around 0.008%. This is due to the $\bar{p}$ drift speed $v_{\mathrm{D}} = en_e\rho/(2\epsilon_0 B)$ (where e and ϵ_0 have their usual meaning) around the axis of the plasma, which gives any $\bar{\mathrm{H}}$ formed a large velocity component in the plane orthogonal to the trap axis, causing a more isotropic emission distribution. This interpretation is confirmed by figure 3, where the density dependence of f_{beam} is shown for five different injection radii and two different magnetic fields. We note that while f_{beam} increases monotonically for injection on axis, for $\rho > 0$ it drops with both density and ρ, as anticipated by the formula for v_{D}. The form of v_{D} also explains why this effect is less pronounced at the higher magnetic field.

We note that $v_{\mathrm{D}} = 90.5 \times (\rho/0.1\ \mathrm{mm}) \times (n_e/10^{14}\ \mathrm{m}^{-3}) \times (1\ \mathrm{T}/B)\ \mathrm{m\,s}^{-1}$, while the axial antiproton speed is $v = 3095\sqrt{0.05\ \mathrm{eV}/E_{\mathrm{in}}}$. Thus, using these speeds, and $E_{\mathrm{in}} = 0.05$ eV, we arrive at $\tan\alpha < 0.1$ for $n_e/(10^{14}\ \mathrm{m}^{-3}) < 3.4 \times (B/1\ \mathrm{T}) \times (0.1\ \mathrm{mm}/\rho)$. We find that this estimate is roughly consistent with the results in figure 3. However, this estimate ignores a number of important factors, such as the thermal component of the velocity, the slowing of the axial velocity due to interaction with the plasma, and the effects of multiple formation/ionisation cycles.

The maximum of the $\rho = 0.1$ mm data around 0.5 eV in figure 2 is not fully understood. However, we have observed that for these parameters, a significant number of $\bar{\mathrm{H}}$s leave the cylindrical plasma through the mantle, rather than the end cap, whilst still satisfying the condition $\tan\alpha < 0.1$. Thus, this behaviour is likely to be a combination of geometrical effects coupled to different velocity distributions and non-isotropic collision dynamics due to the presence of the axial magnetic field. We further note that at 0.75 eV, the $\bar{p}$ speed equals the

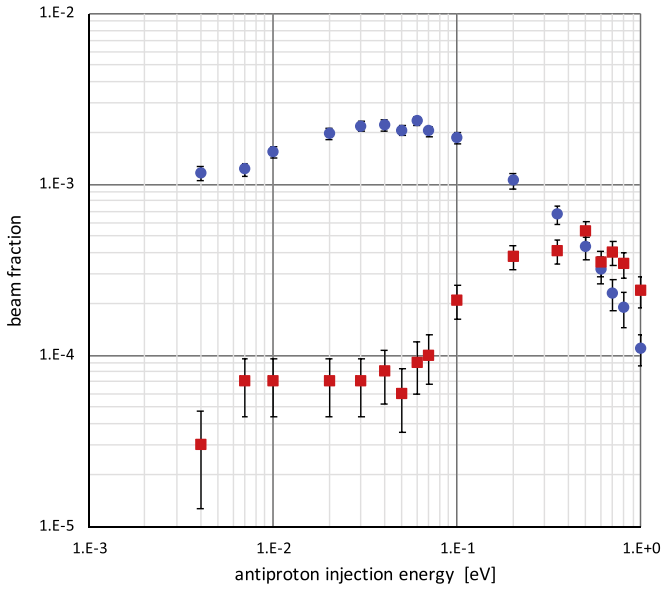

Figure 2. The beam fraction f_{beam}, for $\bar{p}$ injection on axis (blue circles) or 0.1 mm away from the axis (red squares). The data here are for $T_e = 15$ K, $n_e = 10^{15}$ m^{-3} and $B = 1$ T.

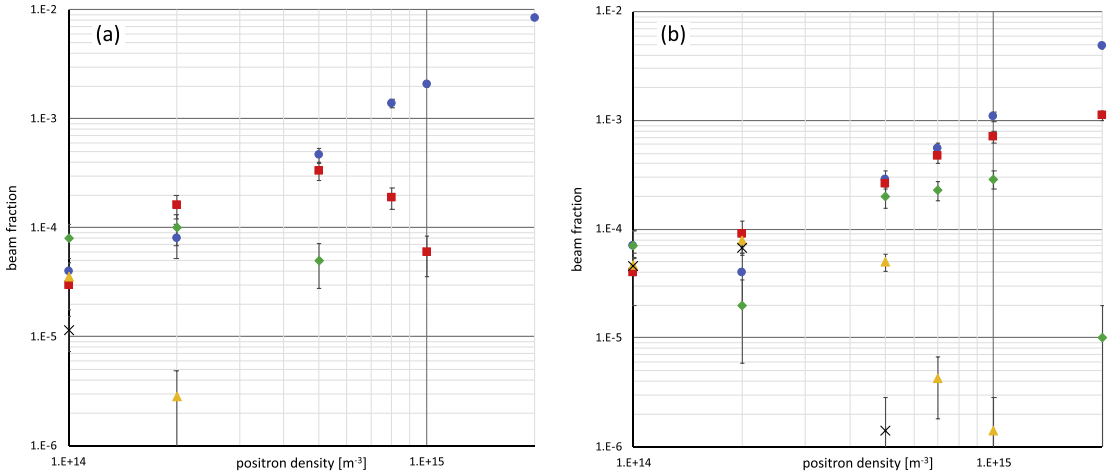

Figure 3. The beam fraction f_{beam}, for $\bar{p}$ injection on axis (blue circles), and for $\rho = 0.1$ mm (red squares), 0.2 mm (green diamonds), 0.5 mm (orange triangles) and 0.8 mm (black crosses), as a function of plasma density. Panel (a): $B = 1$ T, panel (b): $B = 3$ T. In both panels $E_{\text{in}} = 0.05$ eV and $T_e = 15$ K. Missing data points should be interpreted as zero.

average thermal speed of a 15 K positron. This means that the thermal distribution of positrons colliding with the $\bar{p}$ will be Doppler shifted, and the frequency of collisions will increase in the forward direction, while being reduced in the opposite direction, resulting in a greater drag force on the $\bar{p}$s (see figure 9 below). We have not investigated in detail what this means for the $\bar{\text{H}}$ formation process.

One way of increasing the number of $\bar{\text{H}}$s created could be to use a longer plasma [17], and this is investigated in figure 4, where the average $f_{\bar{\text{H}}}$ and f_{beam} per cm of the plasma, for columns between 1 and 10 cm in length (again assuming injection on the axis), are displayed. For plasmas shorter than ~5 cm, both measures increase faster than linear with the length. The reason is that any $\bar{\text{H}}$ formed will need to collide with positrons a number of times in order to reach a binding energy large enough for it to be stable, and this is less likely to happen if the initial formation occurs too close to the end of the plasma. Assuming that an $\bar{\text{H}}$ needs a distance d within the plasma to stabilise, the length of the plasma is l and the fraction of $\bar{p}$ converted to $\bar{\text{H}}$ in 1 cm is f, then the number of $\bar{\text{H}}$ formed per length is $f(l-d)/l$. Fitting this expression to the data in figure 4 gives $d = 0.33$ cm for both sets of data, while $f = 9.4 \times 10^{-3}$ cm^{-1} for $f_{\bar{\text{H}}}$ and 3.3×10^{-3} cm^{-1} for f_{beam}. The fits are displayed along with the data in the figure.

Our condition, $\tan\alpha < 0.1$, for $\bar{\text{H}}$ beam formation is somewhat arbitrary, and for experimental situations will be dependent upon a number of issues. Figure 5 shows the distribution of $\tan\alpha$ for $E_{\text{in}} = 0.05$ eV, $T_e = 15$

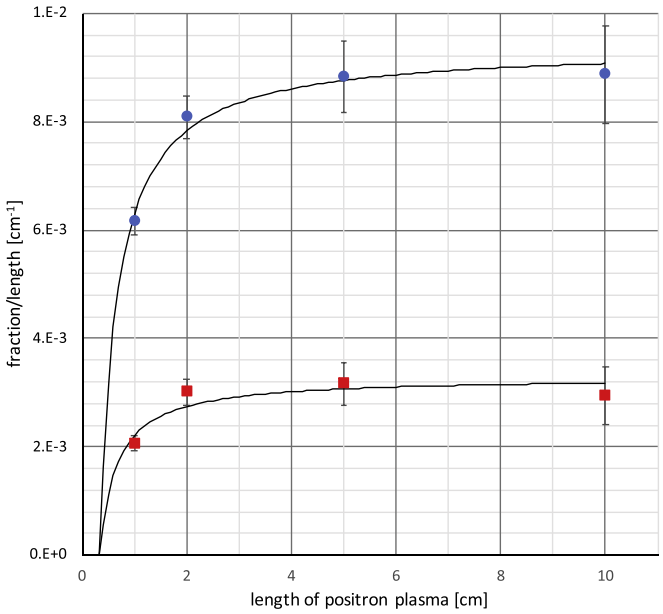

Figure 4. The antihydrogen fraction $f_{\bar{\mathrm{H}}}$ (blue circles) and the beam fraction f_{beam} (red squares) per cm of the plasma, for different plasma lengths. The injection energy was $E_{\mathrm{in}} = 0.05$ eV, $T_e = 15$ K, $n_e = 10^{15}$ m^{-3} and $B = 1$ T. The lines are fits to the simple $f\,(l - d)/l$ model (see text).

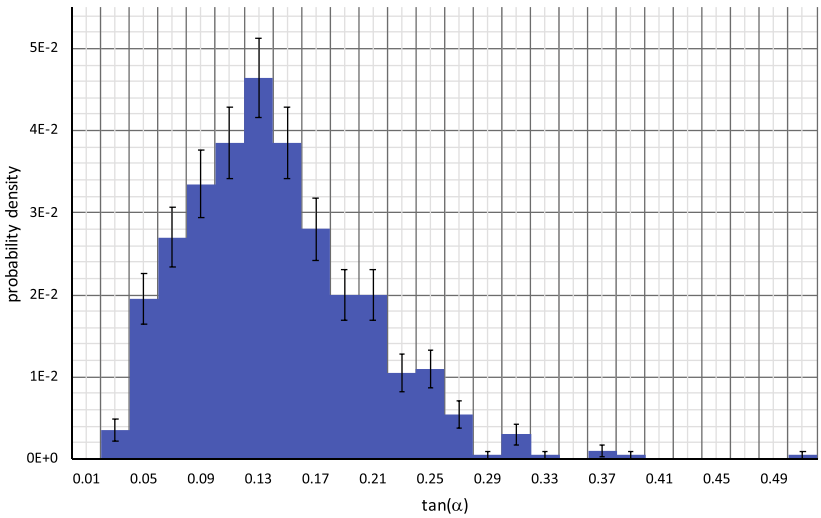

Figure 5. The angular distribution of the emergent $\bar{\mathrm{H}}$, given in terms of $\tan\alpha$ (see text) for $E_{\mathrm{in}} = 0.05$ eV, $T_e = 15$ K, $n_e = 10^{15}$ m^{-3} and $B = 1$ T.

K, $n_e = 10^{15}$ m^{-3}, and $l = 1$ cm (i.e. close to the maximum in figure 1(a)). The deviations from the initial axial velocity are due both to the drift velocity v_{D} (though this should be small for on-axis injection) and the cyclotron motion, as set by the temperature of the antiproton in the plane transverse to the axis. For higher injection energies, this distribution will of course be more peaked in the forward direction, but on the other hand fewer $\bar{\mathrm{H}}$ will be generated. Figure 6 shows how f_{beam} changes for a more strict condition, $\tan\alpha < 0.05$, and also for a larger acceptance $\tan\alpha < 0.2$. As a comparison, in [9, 22] a detector with 10 cm diameter was placed at a 2.7 m distance, which corresponds to $\tan\alpha < 0.019$. We find that the local maximum persists irrespective of which condition is used, though the more strict conditions give reduced yields and poorer statistics in our simulation.

Next, we compare data at the magnetic field of 1 T to results for 3 T. In figure 7 we find an energy-dependent reduction in f_{beam}, by at most a factor of around 2. $f_{\bar{\mathrm{H}}}$ shows a similar reduction. Since the kinetic energy associated with the drift motion is proportional to B^{-2} our interpretation of the results in figure 2 would entail

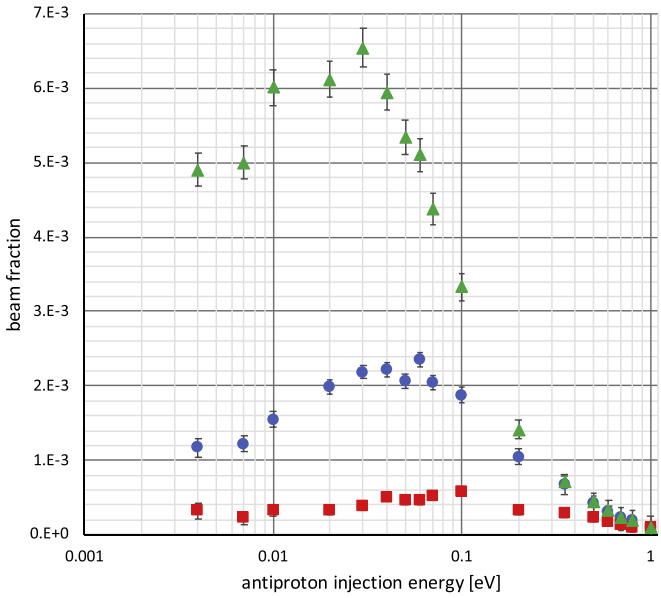

Figure 6. Effect on f_{beam} using three different criteria for $\bar{\mathrm{H}}$ forming the beam; $\tan\alpha < 0.2$ (green triangles); our standard $\tan\alpha < 0.1$ (blue circles), $\tan\alpha < 0.05$ (red squares). Here we used $T_e = 15$ K, $n_e = 10^{15}$ m^{-3} and $B = 1$ T.

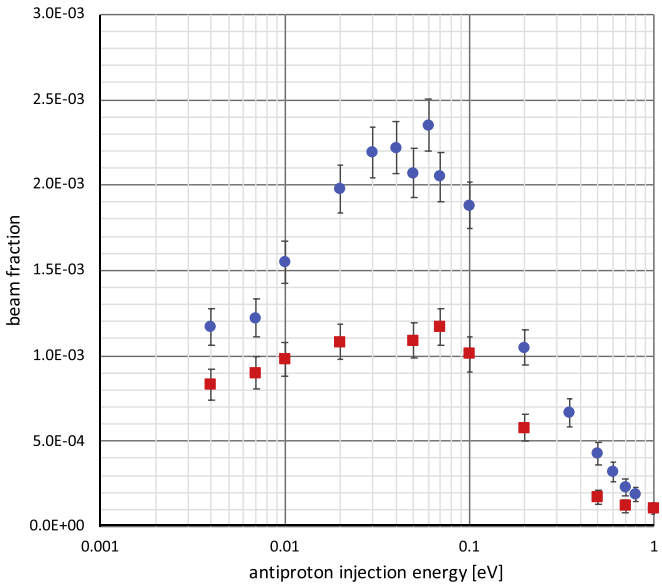

Figure 7. Effect on f_{beam} from a change in the magnetic field from 1 T (blue circles) to 3 T (red squares). Here we use our standard criteria for beam-like $\bar{\mathrm{H}}$, $T_e = 15$ K and $n_e = 10^{15}$ m^{-3}.

that the reduction of f_{beam} with increased injection radius is less pronounced at a higher magnetic field. As shown in figure 3(b) this is indeed the case.

Finally, we examine the properties of the $\bar{\mathrm{H}}$s in the beam. In figure 8 we show how the distribution of binding energies (E_{b}) alters if either E_{in}, n_e or B is changed from our standard set of parameters ($E_{\mathrm{in}} = 0.05$ eV, $n_e = 10^{15}$ m^{-3}, $B = 1$ T, $T_e = 15$ K). In the simulations we only followed the binding energies of the $\bar{\mathrm{H}}$ down to 300 K (here we use kelvin as an energy unit, with conversion to usual energy units given by Boltzmann's constant, that is, 300 K corresponds to 0.026 eV or a principal quantum number $n = 23$), so the distributions below this value are meaningless, and are represented by a single bin. For the standard parameters we find that the $\bar{\mathrm{H}}$s are relatively tightly bound, and well below the 'bottle-neck' energy at $\sim 6k_{\mathrm{B}}T_e$. Reducing the density clearly reduces the typical binding energy. Though statistics are poor, also increasing B or E_{in} seems to have a small effect in the same direction. This is all consistent with the picture that binding energy increases with the number of collisions the $\bar{\mathrm{H}}$s undergo between the initial three-body formation event and the time they leave the plasma. In figure 8 we also show the same data displayed as the fraction of $\bar{\mathrm{H}}$ with principal quantum number

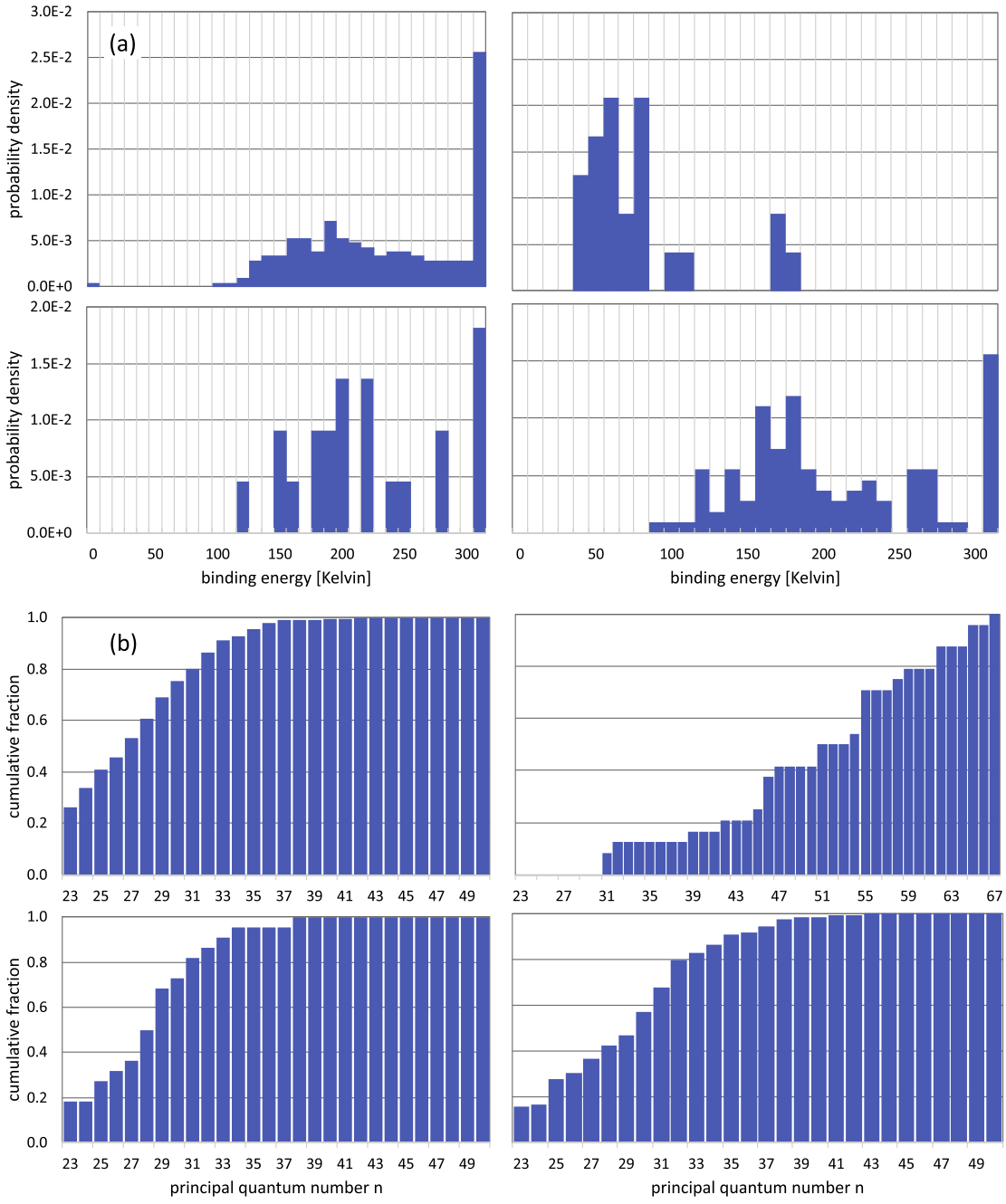

Figure 8. Panel (a): the distribution of binding energies and panel (b): corresponding principal quantum number n of the beam-like (according to our standard definition) emerging $\bar{\mathrm{H}}$. In the upper left frame the same parameters as in figure 2 were used. In the other frames one parameter was changed: $n_e = 10^{14}$ m^{-3} (upper right), $E_{\mathrm{in}} = 1$ eV (lower left), $B = 3$ T (lower right). Binding energies >300 K are represented in a single bin at 300 K. The histograms have been normalised to probability density, but are based on very different numbers of beam-like $\bar{\mathrm{H}}$ (row-by-row, left-to-right): 207, 24, 22, 109.

(defined without consideration of external fields as $n = \sqrt{\mathrm{Ry}/E_{\mathrm{b}}}$, where Ry = 13.6 eV is the usual Rydberg energy) less than a certain value. This corresponds more directly to the data presented in [9], though we do not have enough information for quantitative comparisons. The experimental observation, 99 $\bar{\mathrm{H}}$s with $n < 43$ in a 4950 s run period and 29 with $n < 29$ in 2100 s, corresponds to a detection rate for $n < 29$, which is 69% of that for $n < 43$. This is consistent with the result from our standard set of parameters, though this is probably coincidental as experimental conditions are likely to be different. Nevertheless, the experimental results are clearly inconsistent with our simulation at $n_e = 10^{14}$ m^{-3}, thus pointing to a higher positron density.

Figure 9 shows the change in kinetic energy along the axis. Due to thermal fluctuations (or, on a microscopic scale, the randomness of particle collisions), this property can both increase and decrease. However, overall the average is somewhat reduced, as given enough time the $\bar{p}$ will thermalise with the positron plasma. The figure compares two injection energies, $E_i = 0.05$ eV and $E_i = 1.0$ eV. At the lower injection energy the reduction is small compared to the spreading, on average the kinetic energy is reduced by only -0.45 meV for the beam-like

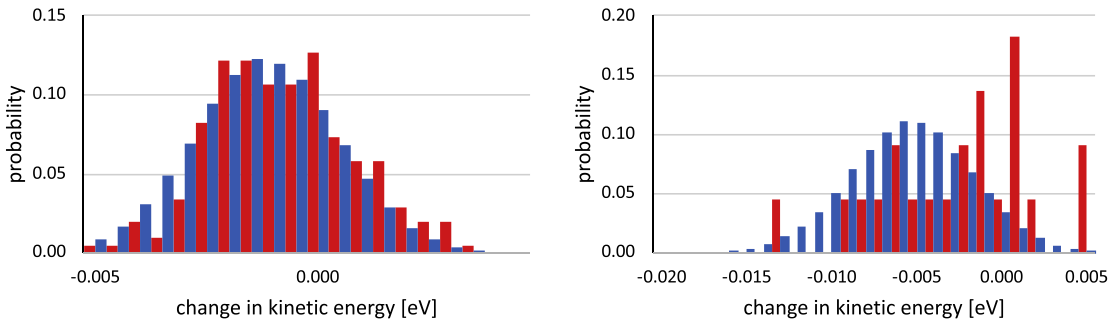

Figure 9. The distribution of change in kinetic energy along the beam axis of the beam-like (according to our standard definition) emerging $\bar{\mathrm{H}}$ (red), and of all emerging $\bar{p}$ (blue) In the left graph $E_i = 0.05$ eV, in the right graph $E_i = 1.0$ eV. In both panels, $T_e = 15$ K, $n_e = 10^{15}$ m^{-3} and $B = 1$ T.

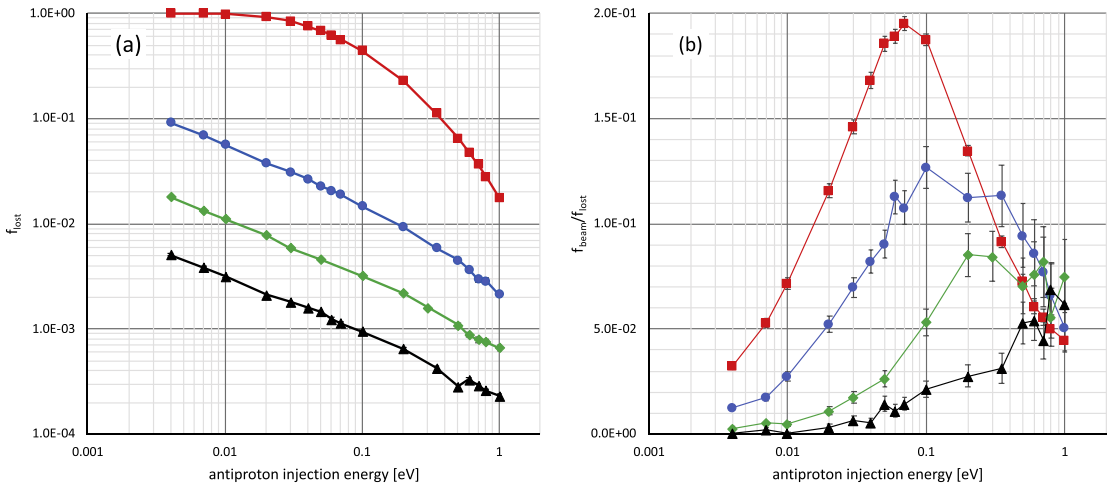

Figure 10. Panel (a): the fraction f_{lost} of $\bar{p}$ lost from the formation process for a single pass through the plasma (see text). Panel (b) fraction of $\bar{p}$ giving rise to beam-like $\bar{\mathrm{H}}$, divided by the fraction lost. Parameters (including colour coding of temperatures) as in figure 1, i.e. $n_e = 10^{15}$ m^{-3}, $l = 1$ cm and $B = 1$ T. The lines are drawn to guide the eye.

$\bar{\mathrm{H}}$, and -1.0 meV for all $\bar{p}$. Since the initial kinetic energy was 0.05 eV, this corresponds to a reduction of 0.9% and 2.0% respectively, in a single pass taking about 3.2 μs. For the higher injection energy the opposite is true. Here the average reduction for all (beam-like) $\bar{\mathrm{H}}$ is 5 meV (2 meV) corresponding to 0.5% (0.2%) in about 0.7 μs.

3.1. Multiple passes

So far, we have presented results for a single pass of the $\bar{p}$s through the positron plasma. This corresponds to the situation simulated in [17], though in that paper the $\bar{p}$s were assumed to have instantly thermalised with the positrons. In the experiment [9], however, the $\bar{p}$s could pass multiple times through the plasma, and whilst we have not simulated this directly, some information can be obtained by considering the $\bar{p}$s after a single pass. We assume that any $\bar{p}$s (whether coming from field-ionisation during the 1 μs wait time, or leaving the positrons as a bare $\bar{p}$) at a trap radius less than that of the plasma (1 mm) can be reflected back into the plasma. However, as shown in figure 2, f_{beam} drops dramatically for $\bar{p}$ outside a certain density-dependent radius. Therefore we assume that all $\bar{p}$s ending up outside this radius are lost from $\bar{\mathrm{H}}$ formation, such that at $n_e = 10^{15}$ m^{-3} we take any $\bar{p}$s ending up at a trap radius $\geqslant$0.1 mm as being effectively removed from formation of beam-like $\bar{\mathrm{H}}$. We denote this fraction f_{lost}. A relevant measure is then $f_{\mathrm{beam}}/f_{\mathrm{lost}}$, or the number of beam-like $\bar{\mathrm{H}}$ generated per $\bar{p}$ lost from the process.

In figure 10 we show f_{lost} and $f_{\mathrm{beam}}/f_{\mathrm{lost}}$ for various parameters. At 5 K f_{lost} is close to unity below $E_{\mathrm{in}} = 0.02$ eV, meaning that the vast majority of $\bar{p}$s form $\bar{\mathrm{H}}$ at least once while traversing the plasma, and hence either form part of the beam, or in a single pass are radially transported out of the region where beam formation is effective. At higher E_{in}, f_{lost} drops as the $\bar{p}$ are less likely to be deflected, which is both due to a smaller probability of $\bar{\mathrm{H}}$ formation and a larger axial velocity. We also find that $f_{\mathrm{beam}}/f_{\mathrm{lost}}$ drops with T_e (except possibly at the highest E_{in} considered), and goes through a broad maximum as a function of E_{in} for all temperatures. This

maximum reflects the maximum of $f_{\rm beam}$ in figure 1(a), but is further reinforced at low energies because $f_{\rm lost}$ increases with reduced $E_{\rm in}$.

As an example, we take a $\bar{p}$ injected with 0.05 eV kinetic energy on the axis of a $T = 15$ K, $n_e = 10^{15}\,{\rm m}^{-3}$, $B = 1$ T, $l = 1$ cm plasma. In a single pass a fraction $f_{\rm beam} = 2.1 \times 10^{-3}$ of the $\bar{p}$ are converted into beam-like $\bar{\rm H}$s, while a fraction 2.3×10^{-2} of the $\bar{p}$s are lost from $\bar{\rm H}$ formation (including those in $f_{\rm beam}$). If these parameters remain constant it would take 30 passes though the plasma before 50% of the $\bar{p}$s are lost. During this process 4.2% of the $\bar{p}$ would be converted into beam-like $\bar{\rm H}$. However, this does not take into account that the kinetic energy of the $\bar{p}$s will change for every pass, nor that $\bar{p}$s can also be lost by trapping in the electrostatic side wells of the Penning traps used to confine the positrons and antiprotons.

We noted in connection with figure 9 that for these parameters the average kinetic energy is reduced by about 2% in a single pass, thus within the 30 passes the $\bar{p}$s would have lost a significant fraction of their axial kinetic energy, though have not yet thermalised with the plasma. To fully explore this effect would require a more elaborate simulation.

4. Conclusions

Our simulations show that radial $\bar{p}$ transport has an important effect on the formation of antihydrogen beams via antiproton–positron interactions. While we have not simulated the cascade of $\bar{\rm H}$ after leaving the plasma, our results show that while the $\bar{p}$ traverse the positron plasma they are significantly deflected. The mechanism is mainly formation of $\bar{\rm H}$, which was investigated in [14]. At very high injection energies, the $\bar{\rm H}$ production becomes more directional, but the yield is drastically reduced. Within the parameter range explored, the largest fraction of $\bar{p}$s converted to beam-like $\bar{\rm H}$s in a single pass through a 1 cm long positron plasma was about 13% (at $T_e = 5$ K, $n_e = 10^{15}\,{\rm m}^{-3}$, $B = 1$ T, $E_{\rm in} \simeq 0.05$ eV), while at the same time about 60% of the $\bar{p}$s were lost from the formation process, and thus cannot contribute to $\bar{\rm H}$ formation through multiple passes through the plasma.

The drift speed $v_{\rm D}$, and hence the radial transport, may be reduced either by reducing the density, or increasing B. Our results show that for on-axis injection both methods instead reduce $f_{\rm beam}$, simply because fewer $\bar{\rm H}$s are formed. This effect does, however, depend on the radius at which the $\bar{p}$s are injected. There is likely to be an experimentally determined distribution of this parameter, and it is therefore impossible to find an optimum from simulations alone. A better strategy is to increase the length of the plasma, though this possibility will be restricted by technical limitations, especially if a high positron density is to be maintained.

It is also notable that we find that there is a broad distribution of atomic states formed, with binding energies in the range of 10s–100s K. Notwithstanding beam-like emission, this will have further consequences for experiment if work on the hyperfine transitions of the ground state is to be contemplated [21, 23]. When further experimental information becomes available, such as plasma densities and temperatures, and if-and-when the $\bar{p}$ injection properties are controlled and known, the simulations reported here can be used to give a useful practical guide on the formation of $\bar{\rm H}$ beams via positron–antiproton interactions.

Acknowledgements

SJ wishes to acknowledge the Swedish Research Council (VR) for financial support, and the High Performance Computing Center North (HPC2N) for computing resources. MC is grateful to the EPSRC (UK) for support of his antihydrogen work.

ORCID iDs

S Jonsell https://orcid.org/0000-0003-4969-1714
M Charlton https://orcid.org/0000-0002-9754-1932

References

[1] Ahmadi M *et al* 2018 *Nature* **557** 71
[2] Ahmadi M *et al* 2018 *Nature* **561** 211
[3] Ahmadi M *et al* 2017 *Nature* **548** 61
[4] Andresen G B *et al* 2010 *Nature* **468** 673
[5] Andresen G B *et al* 2011 *Nat. Phys.* **7** 558
[6] Gabrielse G *et al* 2012 *Phys. Rev. Lett.* **108** 113002
[7] Eriksson T 2009 *Hyperfine Interact.* **194** 123
[8] Ahmadi M *et al* 2017 *Nat. Commun.* **8** 681
[9] Kuroda N *et al* 2014 *Nat. Commun.* **5** 3089

[10] Testera G *et al* 2015 *Hyperfine Interact.* **233** 13
[11] Pérez P *et al* 2015 *Hyperfine Interact.* **233** 21
[12] Charlton M 1990 *Phys. Lett.* A **143** 143
[13] Maury S *et al* 2014 *Hyperfine Interact.* **229** 105
[14] Jonsell S, Charlton M and van der Werf D P 2016 *J. Phys. B: At. Mol. Opt. Phys.* **49** 134004
[15] Jonsell S and Charlton M 2018 *New J. Phys.* **20** 043049
[16] Radics B, Murtagh D J, Yamazaki Y and Robicheaux F 2014 *Phys. Rev.* A **90** 032704
[17] Radics B and Yamazaki Y 2016 *J. Phys. B: At. Mol. Opt. Phys.* **49** 064007
[18] Gerber S 2018 *J. Phys. B: At. Mol. Opt. Phys.* **51** 035008
[19] Jonsell S, van der Werf D P, Charlton M and Robicheaux F 2009 *J. Phys. B: At. Mol. Opt. Phys.* **42** 215002
[20] Hurt J *et al* 2008 *J. Phys. B: At. Mol. Opt. Phys.* **41** 165206
[21] Sauerzopf C *et al* 2016 *Hyperfine Interact.* **237** 103
[22] Nagata Y *et al* 2016 *Nucl. Instrum. Methods* A **840** 153
[23] Diermaier M *et al* 2017 *Nat. Commun.* **8** 15749